3.2 Results and Discussion for α_q and Γ_φ

This section deals with the experimental analysis and results for the analog to Faraday's Induction Disc. The sample had a critical zero field transition temperature of $T_c = 88$ K. The transition temperature, defined as the peak of the $dR(T,B=0)/dT$ curve. (see figure 3.3a). A transition temperature, $T_c(H)$, for the magnetic field resistivities is defined as $dW(T,B)/dT$, the following values for the 4 fields used are: 0.59 T – **87.5 K**; 1.78 T – **86 K**; 3.55 T – **84 K**; 8.29 T – **81.5 K**. The sample displayed negligible resistive broadening for the different applied currents, with and without applied magnetic field. The broadening due to the applied magnetic field, associated with the depinning of vortices, is indicated in figure 3.3b, for all fields and an applied current of 100 mA.

According to the procedures set out in section 3.1, the 12 current/field configurations are analysed to determine $\alpha_q(T)$ and $\Gamma_\varphi(T)$. The contact pairs were situated on four imaginary perpendicular radial lines with varying distances between the two corresponding contacts. Table 3.1 overleaf, gives the different radial distances as well as the d(R), D(R) functions necessary for the analysis. In equation 3.6 the value of $\mathbf{w_n}$ is found by extrapolating a function describing the behaviour of the W(T) curves in the normal state. Instead of the usual linear extrapolation, a quadratic dependence of the form, $A + BT + CT^2$, is fitted to describe the data. It is found for this particular sample that the quadratic temperature dependence is a better approximation to the normal–state data (see APPENDIX B). With regard to the normal state analysis in high–T_c materials, there is evidence that thermodynamic fluctuations are present in the sample for temperatures as high as $2T_{co}$, which can contribute significantly to the shape of the metallic region.[64] For YBCO in particular, the relative oxygen content (section 1.2.2.1) can produce significant changes in the characteristics of the $R_N(T)$ curve, (normal–state resistance). Ausloos et al[64] discuss the premature rounding of the res[illegible]ve curve close to the transition temperature

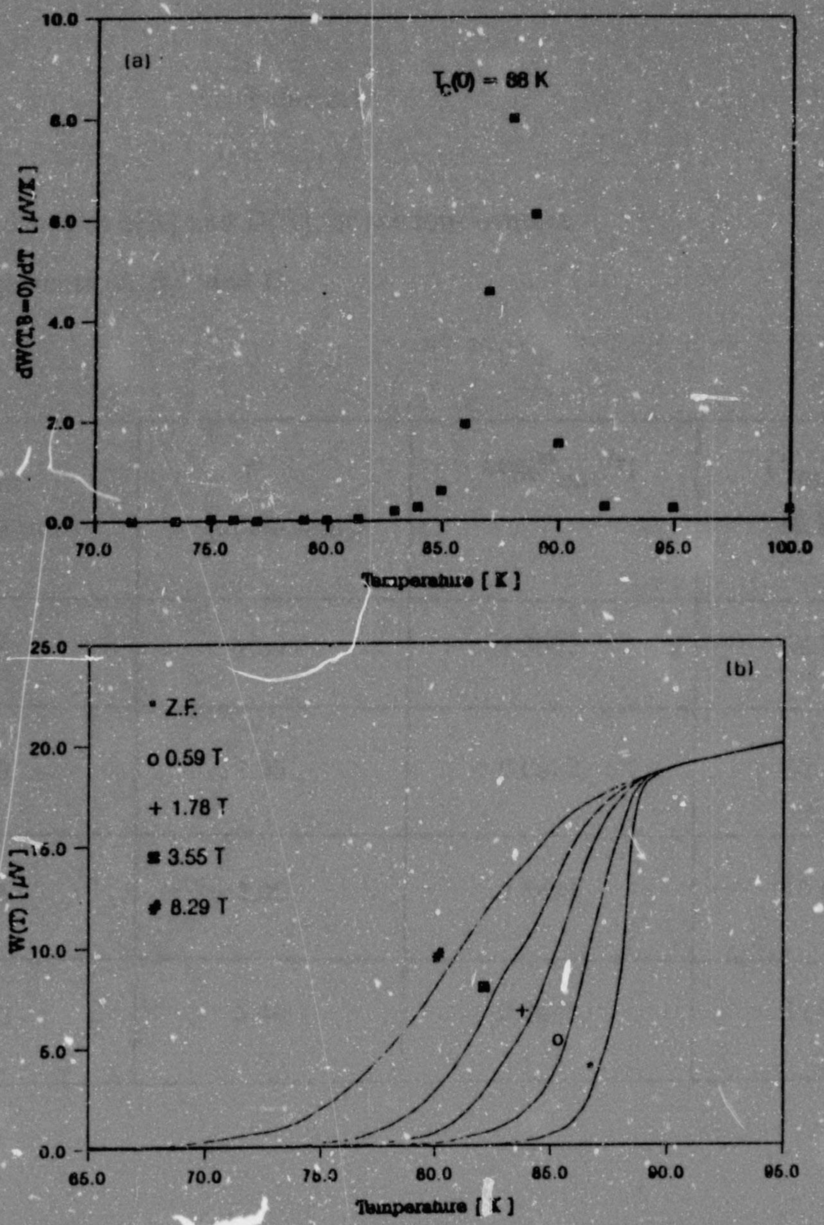

Figure 3.3 (a) $dW(T,B=0)/dT$ for 30 mA, the three currents used displayed no resistive broadening and hence $T_c(B=0)$ was taken as 88 K

(b) The resistive broadening of the four fields used: 0.59, 1.78, 3.55 and 8.29 T with a current of 100 mA.

Table 3.1

Dependence of d(R) and D(R) for the four contact arrangements; A,B,C and D.

R_{out} ($\pm$0.05 mm)	r ($\pm$0.05 mm)	$Log[R_{out}/r]$	$(R_{out}^2 - r^2)$ ($\pm$0.10 mm^2)
4.35	1.60	1.0002	16.36
4.50	2.25	0.6932	15.19
4.85	2.80	0.5494	15.68
4.80	3.40	0.3448	11.48

and show how it can add to the curvature of the normal state resistivity. The resulting normal state behaviour, $w_n(T)$ for each contact pair is proportional to the radial function $d(R) \equiv \log(R_{out}/r)$. Figure 3.4 represents an example of this dependency where a straight line is fitted to the four points. The correlation coefficient, r = 0.989, is an indication of the accuracy of the linear regression. The slope of the straight line corresponds to the other parameters in equation 3.2. Applying equation 3.6 to the induced voltage data for each contact pair, and with the fitted data w_n, 4 points result when $W(T)_i/w_{ni}(T)$ is plotted as a function of $(R_{out}^2 - r^2)_i/w_{ni}(T)$, $1 \leq i \leq 4$, for all the temperatures. The straight lines fitted for each temperature represent good fits with correlation coefficients between 0.89 and 0.99 for temperatures in the range 60 K $\leq T \leq$ 100 K (the region of interest). Figure 3.5 shows lines fitted to the data of the contact points at 5 different temperatures for 10 mA and 0.59 T. The functional dependence of Γ_φ, $D(R) \equiv (R_{out}^2 - r^2)$, is therefore correct, since any incorrect form of D(R) would result in curvature between the 4 points. The slopes of the lines for each temperature are exactly $\Gamma_\varphi(T,J,B)$, and exist in the interval, $0 \leq \Gamma_\varphi \leq \Gamma_{\varphi max}$, (where $\Gamma_{\varphi max}$ is the peak value for each $\Gamma_\varphi(T,J,B)$). The lines have slope of zero in two cases: for low temperatures where vortices are pinned and no substantial vortex rotation occurs; for temperatures > T_c where the pair – breaking mechanisms are maximised and dissipation only occurs due to quasi–particle scattering processes. Between these extreme regions, the flux motion assumes a maximum value corresponding to the largest contribution from the inductive voltage. The intercept of the fitted line with the $R_{out} = r$ line gives values for $\alpha_q(T)$. This value represents an averaged α_q for all four contact pairs. Figure 3.6a depicts the results for the 100 mA current for two fields, 1.78 T and 8.29 T. From the behaviour of α_q, it is apparent that the half–maximum value corresponds to a temperature, $T_c(B)$ defined as dW(T,B)/dT (see above). The curves for $\alpha_q(T)$ show no current dependence, (figure 3.6b), however, this may be due to the fact that all currents used were within the low current regime.

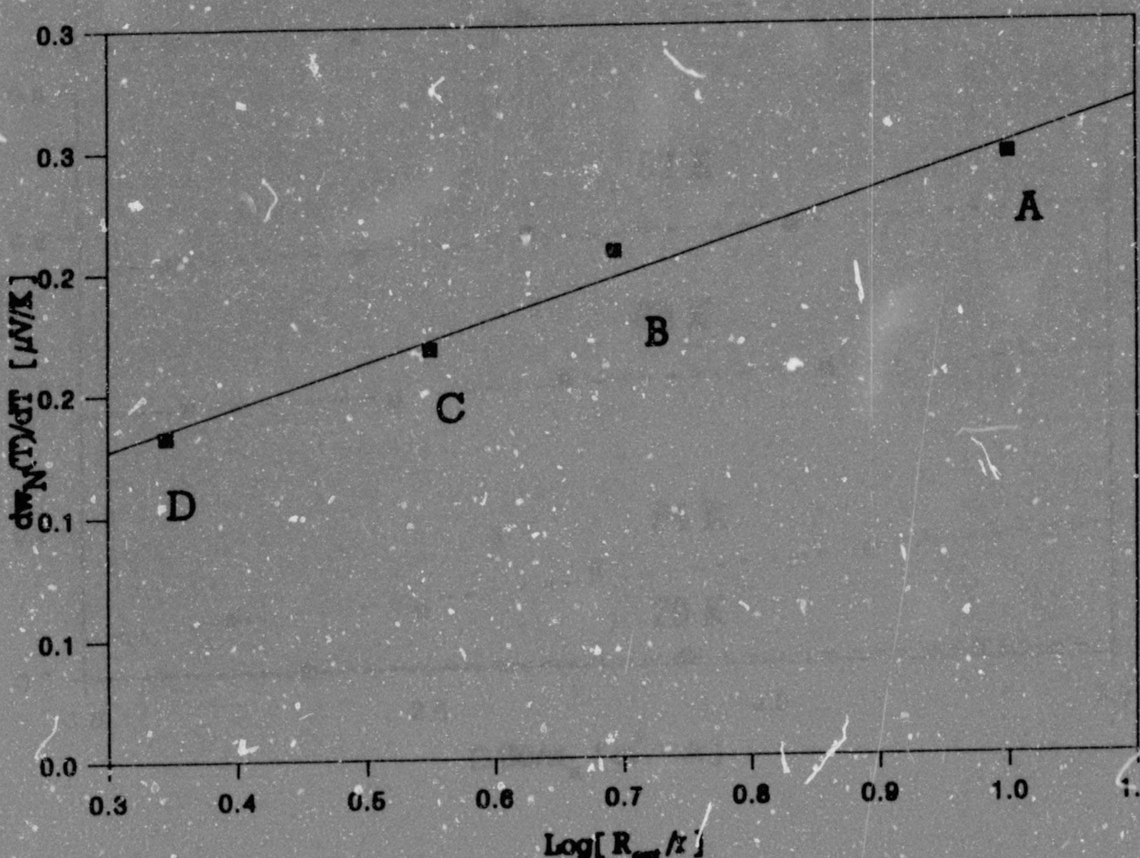

Figure 3.4 Functional dependence $d(R) \equiv \mathrm{Log}[R_{out}/r]$, is illustrated by plotting the temperature derivative of the normal–state $dw_N(T)/dT$, versus $d(R)$ for each contact pair. For 10 mA/0.59 T, the correlation coefficient of the fit is, $r = 0.989$.

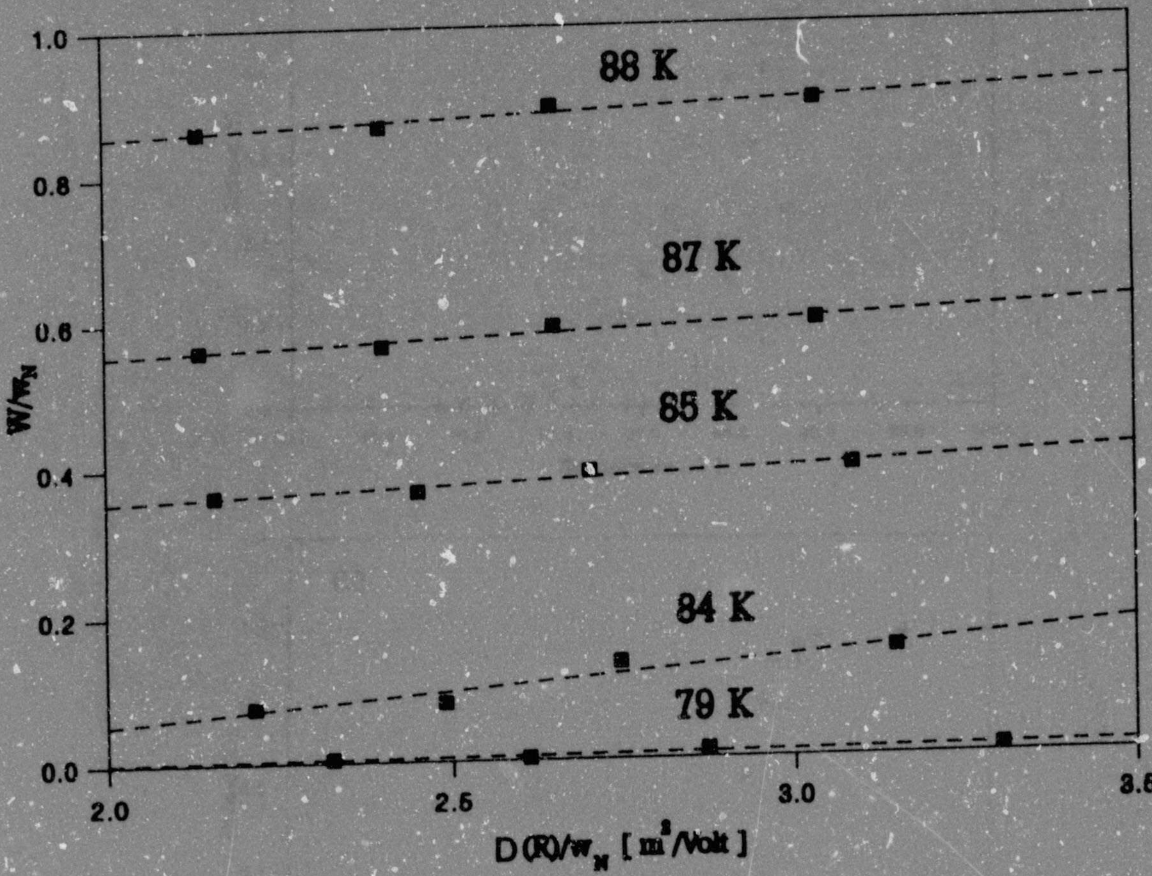

Figure 3.5 $W(T)/w_N(T)$ versus $(R_{out}^2 - r^2)/w_N(T)$ for 10 mA, 0.59 T at five discrete temperatures. The intercepts of the lines with the ($R_{out} = r$) axis yield the value for $\alpha_q(T)$. The notable change in gradient of the lines is exactly the dependence of $\Gamma_\varphi(T)$, varying between zero and some maximum value. The straight line extrapolation for each temperature indicates the validity of the D(R) dependence.

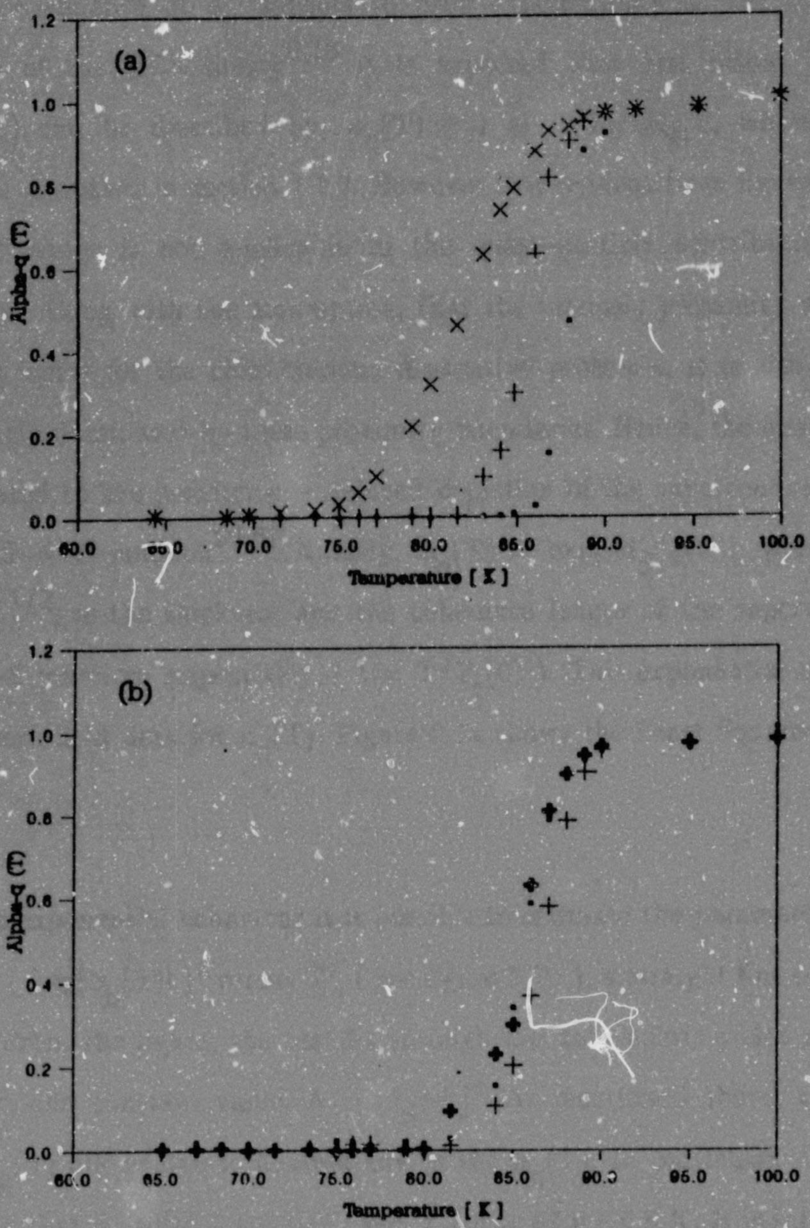

Figure 3.6 (a) Temperature dependence of α_q, for 100 mA and magnetic fields: 0 T, [·]; 1.78 T, [+] and 8.29 T, [×].

(b) Current independence of $\alpha_q(T)$ for 10 [·], 30 [+] and 100 mA [+]. This feature may be a result of low current densities used in the study.

The temperature dependence of α_q appears to drop exponentially as the temperature decreases. In view of the BCS theory,[6,16] it is expected that just below $T_c(0)$, the behaviour of $\alpha_q(T)$ can be described by, $\alpha_q(T) \cong 1 - \Delta(T)/2K_BT$, where $\Delta(T) = \Delta_o(1-T/T_c)^{1/2}$, as discussed in section 1.1.2. However it is evident from figure 3.6a that the power–law behaviour is not applicable to the quasi–particle contribution in this particular geometry. Along with the assumption, that the intrinsic proximity weak–links are the influencing factor for the characteristic dissipative processes, it is also concluded that $\alpha_q(T)$ is strongly dominated by these proximity boundaries. Hence, the quasi–particle contribution is related to the proximity – induced depletion of the superconducting order parameter near a S–N–S junction.[26,67] Namely, $\alpha_q(T) = \exp[-d_S/\xi(T)]$, where d_S and $\xi(T) = \xi_o\cdot(1-t^2)^{-1/2}$, is the thickness and the coherence length of the superconducting region of the S–N–S junction, respectively, ($t = T/T_c(0)$). This exponential dependence is used to fit the zero field data for $\alpha_q(T)$. Figure 3.7a shows the Least Squares fit to the 100 mA data.

In the region of the exponential behaviour it is possible to estimate the parameters, d_S and $T_c(0)$. By plotting ($\mathrm{Log}[\alpha_q(T)]$)^2 versus T^2, (see figure 3.7b), a straight line of the form, $A - BT^2$, results. From the figure, the best fit through the data points yields a gradient, $B = [d_S/\xi_oT_c(0)]^2$, and constant value, $A = [d_S/\xi_o]^2$. As mentioned above, the current independence of $\alpha_q(T)$ allows one to analyse any of the $\alpha_q(T)$. In particular, for the 100 mA data it is found that $d_S \simeq [16.1 \pm 0.1]\cdot\xi_o$ and $T_c(0) = 87.9 \pm 0.3$ K. It is interesting to note that this method of estimating $T_c(0)$, produces a result similar to the peak of the dW/dT curve, for zero field, (see figure 3.3a). Returning to figure 3.7a, the fact that the fit to $\alpha_q(T)$ does not reach unity at $T = T_c(0)$, indicates that there exists a region of strong fluctuations in the vicinity of the zero field transition temperature.

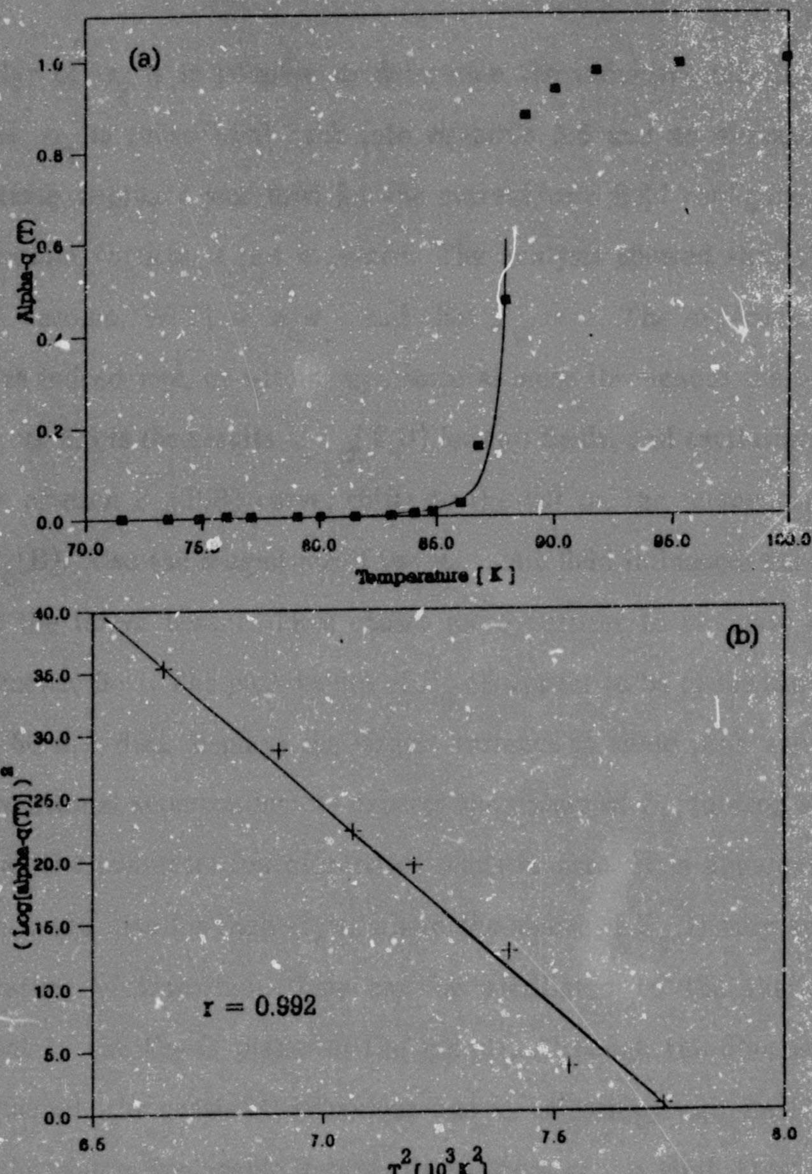

Figure 3.7 (a) Least Squares fit of $\alpha_q(T) = \exp[-d_S/\xi(T)]$ to the 100 mA data. The fact that the $\alpha_q(T)$ data does not reach unity at $T_c(0)$, indicates that fluctuations are prevalent in the vicinity of $T_c(0)$. Solid line is exponential fit to data below $T_c(0)$.

(b) A plot of ($\mathrm{Log}[\alpha_q(T)]$)^2 versus T^2, for 100 mA . The linear regression produces an intercept, $A = [d_S/\xi_o]^2$ with slope, $B = [d_S/\xi_o T_c(0)]^2$, which provides estimates of the superconducting layer, $d_S = [16.1 \pm 0.1]\cdot \xi_o$ and critical temperature $T_c(0) = 87.9 \pm 0.8$ K.

With the knowledge of α_q it is possible to determine the inductive dissipation due to circulating vortices. α_q is substituted back into equation 3.6 and an average for Γ_φ is determined. The same approach was used for the current/zero field configurations where the existence of mobile vortices is not expected. The analysis showed that the form of equation 3.6 must become, $W(T) = \alpha_q w_n$, and that $\Gamma_\varphi = 0$. The experimental results verified that Γ_φ was indeed zero, or within experimental noise throughout the temperature region studied. Figure 3.8 is the results of $\Gamma_\varphi(T,B)$ for two fields, and excitation current of 100 mA. The peak of each $\Gamma_\varphi(T,B)$ curve, shifts to the left on the temperature scale in accordance with $T_c(B)$. Also the magnitude of the magnetic field influences the area under each Γ_φ curve, as the larger Lorentz force causes more vortices to circulate and hence, generate a larger electric field. The peak values of Γ_φ all appear to be of the same order for all four fields; the 30 mA data displays the largest variance in these peak values, (6 %). The theory of conventional superconductors expects the values of Γ_φ to drop abruptly to zero after $T_c(B)$, as the concentration of vortices tends to zero. It is apparent from the data that this is not the case for high–T_c's, where the shape of Γ_φ is very symmetrical about the temperature of transition. This can be attributed to the thermodynamic fluctuations inherent in the Cu–O planes of the sample. Although the dimensionality of YBCO has been queried, the quasi–2D behaviour due to anisotropy and small coherence length still makes the system favourable towards fluctuations of this kind. From the $\Gamma_\varphi(T)$ curves for the different fields, it is evident that dissipation due to mobile vortices is still observed for a temperature interval $\Delta T \simeq$ FWHM (full width at half maximum) beyond the critical temperature, $T_c(B)$. Figure 3.9 shows the **current dependence** of Γ_φ where the respective curves are scaled to 100 mA for all three currents, (the field is 1.78 Tesla). The average variation from the expected current dependence is 11.3 %. This current dependence can be found in the relation for $\Gamma_o(J,B)$ where it is directly proportional to I, (figure 3.10, is a plot of $\Gamma_o(J,B = 8.29\ T)$ versus I). This dependence on I might indicate the behaviour of the effective rate of rotation, ν_{eff}, with the excitation current.

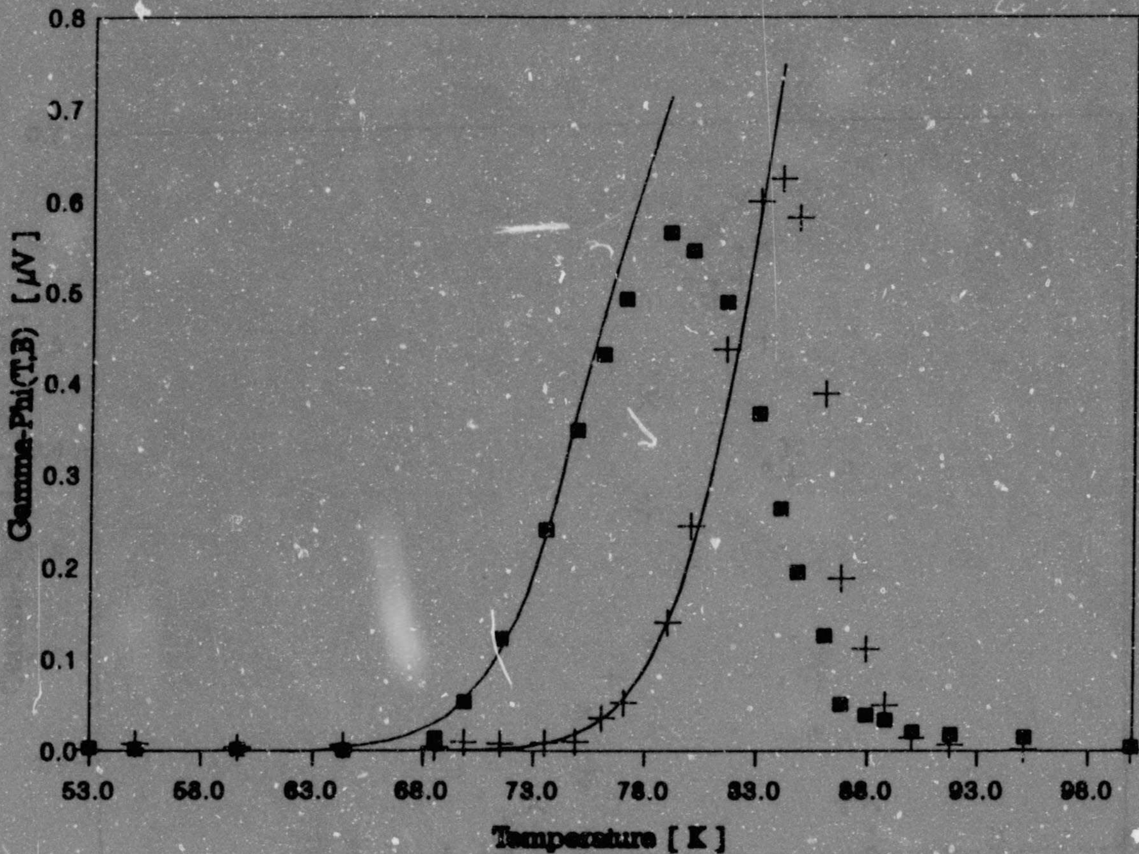

Figure 3.8 Γ_{φ}(T,B) for H = 1.78 T [+] and H = 8.29 T [$\cdot$] with excitation current I = 100 mA. The peak value of Γ_{φ}(T,B) shifts to the left of the temperature scale as the field increases. Also, note symmetry of the curve – suggesting strong fluctuations above T_c(B). Solid curves are the PMTAFF fits to data as described in Section 3.3.

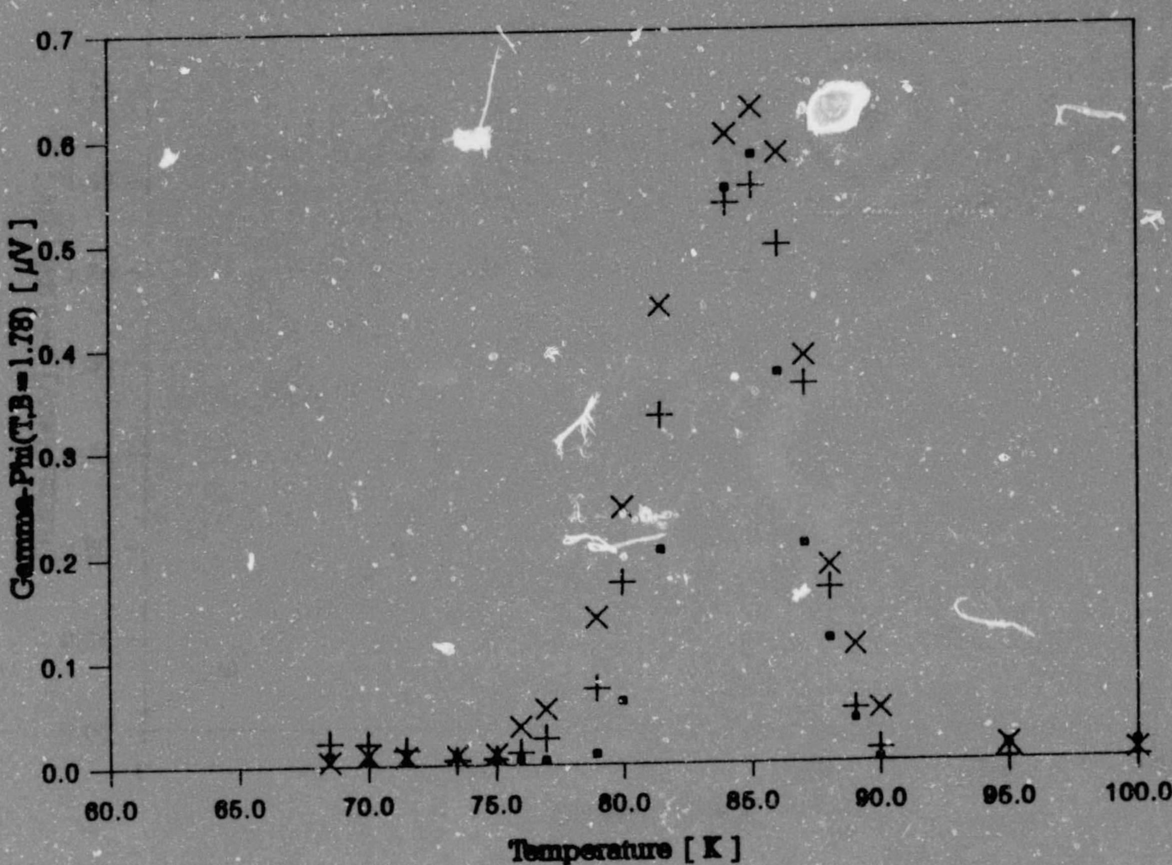

Figure 3.9

Current dependence of $\Gamma_{\varphi}(T,B)$. All three currents have been scaled to 100 mA. The maximum variation from the expected current dependence is 11.3 %. 10 mA [·], 30 mA [+] and 100mA [×].